Mod Rheumatol (2007) 17:115–122
DOI 10.1007/s10165-007-0552-4

ORIGINAL ARTICLE

Hideki Tsuboi · Akihide Nampei · Yoshito Matsui
Jun Hashimoto · Shinichi Kawai · Takahiro Ochi
Hideki Yoshikawa

Celecoxib prevents juxta-articular osteopenia and growth plate destruction adjacent to inflamed joints in rats with collagen-induced arthritis

Received: October 17, 2006 / Accepted: January 12, 2007

Abstract The effect of celecoxib, a selective cyclooxygenase-2 inhibitor, on juxta-articular osteopenia and growth plate destruction adjacent to inflamed joints was investigated in rats with collagen-induced arthritis. Forty rats were assigned to the following six groups: (1) an untreated arthritis group; (2–5) arthritis rats receiving indomethacin (3 mg/kg per day), dexamethasone (0.2 mg/kg per day), or celecoxib (5 or 50 mg/kg per day), and (6) normal control rats. Drugs were administered for 2 weeks from the onset of arthritis. Then the hind paws were measured. Juxta-articular osteopenia and growth plate destruction adjacent to inflamed joints were also assessed using plain radiography, bone mineral density measurement, histology, and histomorphometry. Each treatment reduced inflammation, but only dexamethasone and high-dose celecoxib prevented bone loss adjacent to inflamed joints and significantly decreased bone resorption. In contrast, no treatment affected bone formation parameters. Growth plate destruction adjacent to inflamed joints was prevented by indomethacin, dexamethasone, and high-dose celecoxib. Although dexamethasone abolished inflammation, growth plate destruction was still observed. In conclusion, among the various drugs tested, only celecoxib had a preventive effect on both growth plate destruction and bone loss adjacent to inflamed joints in this arthritis model.

Key words Celecoxib · Growth plate destruction · Juvenile idiopathic arthritis · Juxta-articular osteopenia · Rheumatoid arthritis

H. Tsuboi (✉) · A. Nampei · Y. Matsui · J. Hashimoto · H. Yoshikawa
Department of Orthopaedic Surgery, Osaka University Graduate School of Medicine, 2-2 Yamadaoka, Suita 565-0871, Japan
Tel. +81-6-6879-3552; Fax +81-6-6879-3559
e-mail: h-tsuboi@mx5.canvas.ne.jp

S. Kawai
Division of Rheumatology, Department of Internal Medicine (Omori), Toho University School of Medicine, Tokyo, Japan

T. Ochi
National Hospital Oganization, Sagamihara National Hospital, Sagamihara, Japan

Introduction

Rheumatoid arthritis (RA) is a chronic inflammatory disease that is characterized by synovitis associated with the progressive destruction of cartilage and bone,[1,2] including juxta-articular osteopenia adjacent to inflamed joints and focal erosion of the subchondral bone and joint margins.[3] Recent studies have suggested that both proliferating synovial cells and bone-resorbing osteoclasts play an important role in the bone resorption that occurs at these sites. Juvenile idiopathic arthritis (JIA) is another chronic inflammatory disease that is characterized by arthritis associated with progressive destruction of cartilage and bone that leads to abnormal growth of juxta-articular epiphyses, resulting in joint malalignment and destruction, extremities of different lengths, and short stature.[4]

Nonsteroidal anti-inflammatory drugs (NSAIDs), including indomethacin, are effective anti-inflammatory and analgesic agents that are commonly used to treat RA and JIA, and these drugs decrease the production of prostaglandins (PGs) by direct inhibition of the activity of cyclooxygenase (COX).[5,6] Prostaglandins (PGs) are important inflammatory mediators that are produced at sites of inflammation, including the joints of patients with RA and JIA. Prostaglandins enhance or prolong the effects of various proinflammatory agents and thus aggravate inflammation. Prostaglandins are produced from arachidonic acid by COX,[7,8] and two isoforms of COX are known to exist, which are COX-1 that is constitutively expressed by various cells and tissues[9] and COX-2 that is expressed by inflammatory cells in response to various stimuli.[10]

Previous studies on inflammatory bone conditions have showed that osteoblasts or stromal cells overexpress COX-2, which produces PGs that promote bone resorption. It was also reported that genetically COX-2-deficient mice show impaired bone resorption in response to parathyroid hormone or 1,25-hydroxyvitamin D_3. These findings suggest that COX-2 may have an important role in bone resorption as well as in inflammation, which could be quite distinct from that of COX-1.[11–13]

Selective COX-2 inhibitors are becoming more widely used to treat RA and JIA.[14] These drugs are known to reduce PG production. In addition, celecoxib (a selective COX-2 inhibitor) has been reported to have several effects on bone. Kawaguchi et al.[15] found that COX-2 inhibitors suppress osteoclastogenesis, while Igarashi et al.[16] showed that celecoxib suppresses both bone resorption and osteoclastogenesis in vitro. In addition, Katagiri et al.[17] recently reported that selective COX-2 inhibitors can reduce pannus expansion and joint erosion in a rat model of arthritis. Moreover, Mastbergen et al.[18] reported that celecoxib prevented cartilage damage induced by proinflammatory cytokines in an organ culture system.

These reports have raised the possibility that selective COX-2 inhibitors could prevent juxta-articular osteopenia and growth plate destruction in RA or JIA. Therefore, we investigated the effect of the selective COX-2 inhibitor celecoxib on juxta-articular osteopenia and growth plate destruction in rats with collagen-induced arthritis (CIA), which are commonly used as a model of inflammatory arthritis like RA and develop juxta-articular osteopenia[19] as well as early closure of the juxta-articular growth plates.[20]

Materials and methods

Collagen-induced arthritis model

Collagen-induced arthritis was induced in 6-week-old female Lewis rats (Clea Japan, Tokyo, Japan) using a modification of the method described previously.[21] Rats were anesthetized and immunized intradermally with 0.5 mg of bovine type II collagen (Cosmo Bio, Tokyo, Japan) that had been emulsified in 0.5 ml of Freund's incomplete adjuvant (Difco, Detroit, MI, USA) at 4°C. On day 7, the rats received an intradermal booster injection, which was half the volume of the first dose. The onset of arthritis in the ankle joints could usually be recognized between days 14 and 16, and animals without obvious arthritis by day 16 were excluded from this study. The incidence of arthritis was 70.0% (30 of 43 rats). On day 17, the hind paw volume of each rat was measured with a TK-101 CMP Plethysmometer (Muromachi Machine, Tokyo, Japan), and animals with a hind paw volume greater than 1.65 ml were randomized in equal numbers ($n = 5$ each) to the following five groups: (1) an untreated CIA control group, (2) a group treated with indomethacin at 3 mg/kg per day, (3) a group treated with dexamethasone at 0.2 mg/kg per day, (4) a group treated with celecoxib at 5 mg/kg per day (cele.5), and (5) a group treated with celecoxib at 50 mg/kg per day (cele.50). Five nonimmunized normal control rats were also studied according to the same experimental protocol. All present animal experiments were approved by the institutional review board of Osaka University Graduate School of Medicine.

Drug treatment

Celecoxib was a kind gift from Pharmacia (Skokie, IL, USA), while dexamethasone and indomethacin were purchased from Sigma Chemical Co. (St. Louis, MO, USA). Drugs were prepared as suspensions in 0.5% methylcellulose (Wako, Tokyo, Japan). Rats were treated orally once a day for 2 weeks at the above-mentioned doses with a dosing volume of 0.5 ml/day. Administration was begun on day 17 of the study and continued until the final assessment on day 30.

Radiographic evaluation

On day 30, all rats underwent radiography. After being killed with an overdose of ketamine intramuscularly, the lower extremities were resected and the bones were cleaned of adherent tissue. Then the limbs were positioned over a cassette containing X-ray film (Eastman-Kodak, Seattle, WA, USA) and radiographs were obtained with a conventional microradiography unit (M-60, Softex, Tokyo, Japan) at 30 kV and 3 mA for 75 s.

Measurement of bone mineral density (BMD)

The BMD of the proximal one-third of the tibia was measured by a bone densitometer (Lunar PIXImus; Lunar, Madison, WI, USA) using software provided with the instrument. The region-of-interest (ROI) tool was employed to identify the proximal tibia. To eliminate the fibula from the scans, the oval exclusion ROI was positioned over this bone (Fig. 3Aa).[22] All BMD analyses were done by the same investigator (H.T.).

Bone histomorphometry

All rats underwent double fluorescent labeling before being euthanized. On days 23 and 27, tetracycline hydrochloride (20 mg/kg; Sigma) were injected intraperitoneally. Bone specimens were fixed in 70% ethanol, prestained in Villanueva bone stained for 72 h, dehydrated in alcohol and acetone, and embedded in methylmethacrylate. Then the proximal tibia was cut into 5-μm thick frontal sections for histomorphometry of cancellous bone.[23] Measurements were performed at a magnification of ×320 in the secondary spongiosa at 1 mm from the growth plate using Bone Histomorphometric System software (System Supply, Nagano, Japan). The histomorphometric parameters employed in this study were derived from Parfitt et al., and have been approved by an American Society for Bone and Mineral Research (ASBMR) committee.[24] As static parameters, the trabecular bone volume (BV/TV) and trabecular thickness (Tb.Th) were measured. To measure bone formation, the osteoid surface relative to bone surface and the osteoblast surface relative to bone surface were calculated (OS/BS and Ob.S/BS, respectively). To assess bone resorption, the eroded surface and osteoclast surface were quantified

relative to the bone surface (ES/BS and Oc.S/BS, respectively). To determine the effect of each drug on growth plate destruction, the width of the growth plate and the number of osteoclasts relative to the bone surface (N.Oc/BS) were measured.

Statistical analysis

Results are presented as the mean ± SD. Differences were analyzed by using analysis of variance, and $P < 0.05$ was considered to indicate statistical significance.

Results

Hind paw volume

The hind paw volume of the rats was measured with a TK-101 CMP Plethysmometer at weekly intervals. On days 24 and 30, the hind paw volume of drug-treated animals was significantly smaller than that of the untreated CIA control group (Fig. 1).

Juxta-articular osteopenia

Radiography of the knee joint showed that juxta-articular osteopenia was very mild in the cele.50 or dexamethasone groups, while severe juxta-articular osteopenia was seen in the untreated CIA, indomethacin, and cele.5 groups (Fig. 2).

Quantitative evaluation of juxta-articular osteopenia by measuring the BMD of the proximal one-third of the tibia (Fig. 3Aa) showed that BMD was significantly higher in the cele.50 group (mean ± SD: 0.183 ± 0.02 g/cm^2) and the dexamethasone group (0.247 ± 0.09 g/cm^2) than in the untreated CIA rats (0.155 ± 0.05 g/cm^2). However, there was no significant difference of BMD between the indomethacin group (0.155 ± 0.01 g/cm^2) or the cele.5 group (0.166 ± 0.02 g/cm^2) and the untreated CIA rats (0.155 ± 0.05 g/cm^2) (Fig. 3Ab). Histomorphometric analysis gave results consistent with the BMD data because decrease of BV/TV and Tb.Th were significantly suppressed in the cele.50 group (13.6% ± 3.15% and 48.1 ± 5.43 μm, respectively) and the dexamethasone group (22.8% ± 6.43% and 56.9 ± 4.56 μm) than in the untreated CIA group (5.32% ± 1.53% and 34.0 ± 5.14 μm). This protective effect of high-dose celecoxib and dexamethasone against bone loss in CIA rats was accompanied by a significant decrease of ES/BS (cele.50 and dexamethasone: 20.6% ± 6.37% and 11.6% ± 3.33%, respectively) and Oc.S/BS (6.92% ± 3.02% and 3.43% ± 1.39%), which are bone resorption parameters, compared with the untreated CIA group (ES/BS 39.4% ± 4.94% and Oc.S/BS 13.5% ± 5.40%). However, there were no significant changes of bone formation parameters (OS/BS and Ob.S/BS were respectively 28.3% ± 17.2% and 19.7% ± 15.5% for cele.50, 30.4% ± 5.93% and 16.4% ± 3.36% for dexamethasone, and 27.2% ± 12.3% and 17.9% ± 10.8% for untreated CIA). On the other hand, there were no significant differences of any parameters between the indomethacin group (BV/TV, Tb.Th, ES/BS, Oc.S/BS, OS/BS, and Ob.S/BS were 6.64% ± 0.636%, 33.1% ± 1.38 μm, 44.4% ± 0.226%, 18.2% ± 0.58%, 13.4%

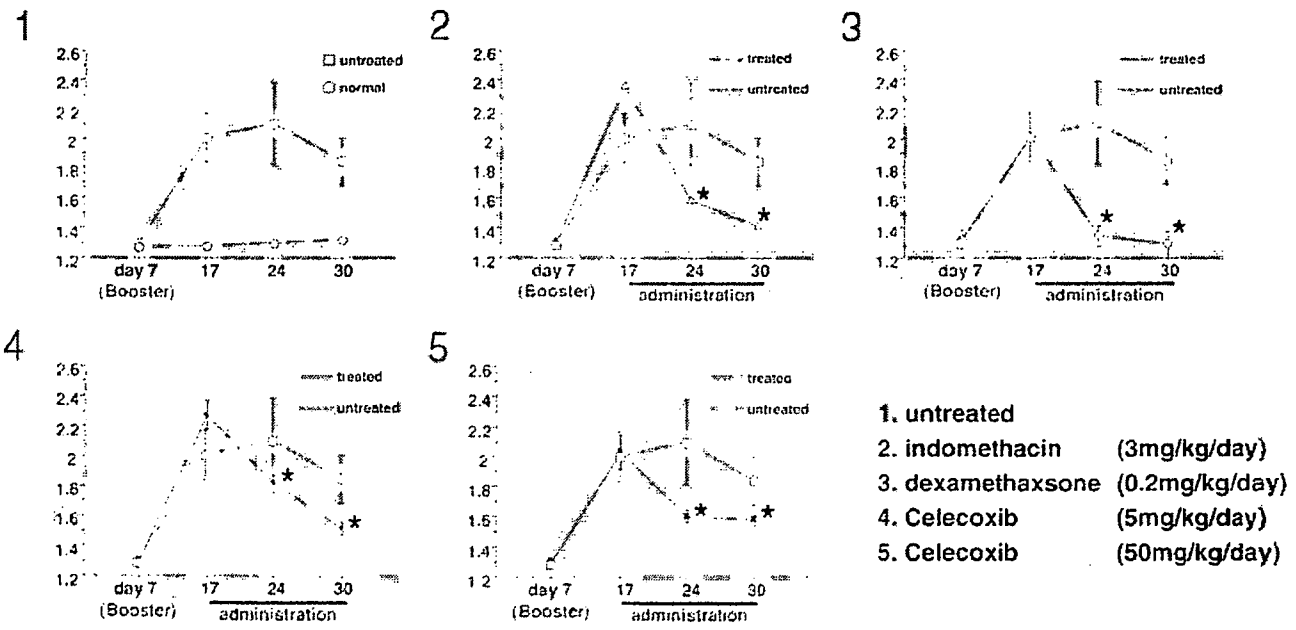

Fig. 1. Effect on the hind paw volume. Each drug significantly improved collagen-induced arthritis (CIA), as evaluated by hind paw volume. Data from five rats in each group were presented as the mean ± SD. *1*, untreated CIA group; *2*, indomethacin group; *3*, dexamethasone group; *4*, cele.5 group; *5*, cele.50 group; *6*, normal control group. On days 24 and 30, the footpad volume in groups 2, 3, 4 and 5 was significantly smaller than in the untreated CIA control group (1). *$P < 0.01$ for the untreated CIA control group vs. each treated group (analysis of variance; ANOVA)

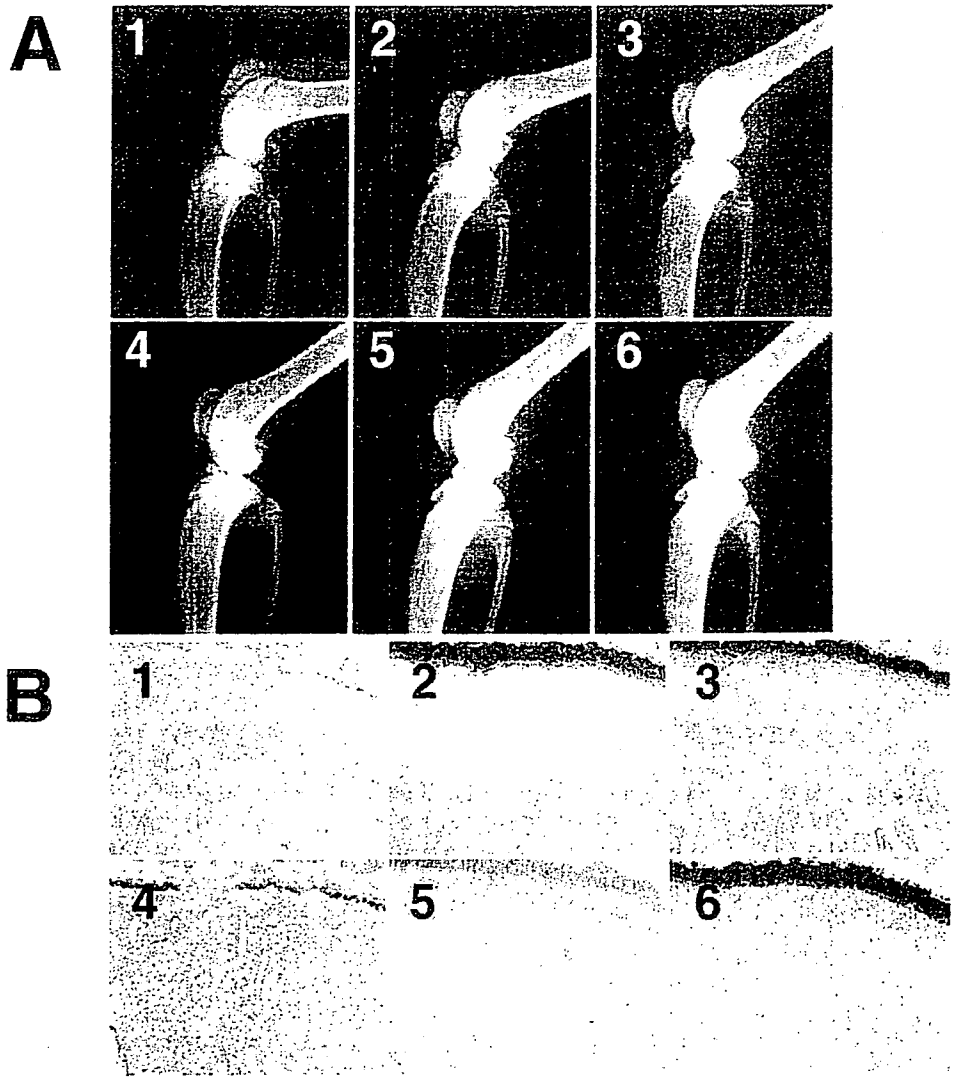

Fig. 2A,B. Effect on juxta-articular osteopenia. **A** Radiographic findings. Representative images selected from the five rats (ten limbs) in each group are presented. *1*, untreated CIA group; *2*, indomethacin group; *3*, dexamethasone group; *4*, cele.5 group; *5*, cele.50 group; *6*, normal control group. Rats from the cele.50 group (5) and the dexamethasone group (3) showed denser juxta-articular bone than untreated CIA rats (1) or rats from the indomethacin group (2) or the cele.5 group (4). An X-ray image of a nonimmunized normal control rat is also shown (6). **B** Histological villanueva bone stained findings. Representative images from the five rats (ten specimens) in each experimental group are presented. Specimens from the untreated CIA group (*1*), the indomethacin group (*2*), and the cele.5 group (*4*) reveal marked loss of bone trabeculae at the proximal tibial epiphysis, as well as the metaphysic, when compared with the nonimmunized normal control rats (*6*). In the cele.50 group (*5*) and the dexamethasone group (*3*), trabeculae are also decreased compared with the non-immunized normal control group (*6*), but are preserved to a certain extent. Original magnification ×40

± 5.43%, and 8.61% ± 5.16%, respectively) or the cele.5 group (6.48% ± 0.757%, 37.0 ± 1.68 μm, 40.3% ± 6.24%, 19.1% ± 6.27%, 24.7% ± 9.21%, and 14.4% ± 9.69%) and the untreated CIA rats. Bone histomorphometry revealed the following values in normal control rats. BV/TV, Tb.Th, ES/BS, Oc.S/BS, OS/BS, and Ob.S/BS were 28.3% ± 3.46%, 55.9 ± 4.65 μm, 29.7% ± 3.00%, 12.5% ± 1.01%, 31.1% ± 5.9%, and 22.2% ± 5.21%, respectively.

Growth plate thickness

Histological examination showed that the growth plate was almost completely preserved in the indomethacin and cele.50 groups, and was partially preserved in the dexamethasone group. In contrast, the growth plate had disappeared in the untreated CIA rats (Fig. 4A, B). Quantitative evaluation of the width of the growth plate showed no significant difference between normal control rats (129 ± 10.7 mm) and the indomethacin group (126 ± 14.1 mm) or the cele.50 group (136 ± 47.7 mm). However, a significant difference was noted between normal rats and the dexamethasone group (61.9 ± 10.0 mm), the cele.5 group (15.2 ± 4.64 mm), and the untreated CIA group (16.1 ± 15.2 mm). The value of N.Oc/BS before administration (on day 17) and in the untreated, indomethacin, dexamethasone, cele.5, and cele.50 groups was 3.21 ± 0.636 no./mm, 2.79 ± 0.636 no./mm, 3.74 ± 0.87 no./mm, 0.640 ± 0.256 no./mm, 4.96 ± 1.92 no./mm, and 1.02 ± 0.694 no./mm, respectively. N.Oc/BS showed a significant difference between before administration (day 17) and the values obtained in the dexamethasone group and the cele.50 group.

Discussion

In this study, we demonstrated an anti-inflammatory effect of high-dose celecoxib (50 mg/kg per day), as well as an inhibitory effect on juxta-articular osteopenia, which was mainly due to decreased bone resorption according to the histomorphometric findings. High-dose celecoxib also pre-

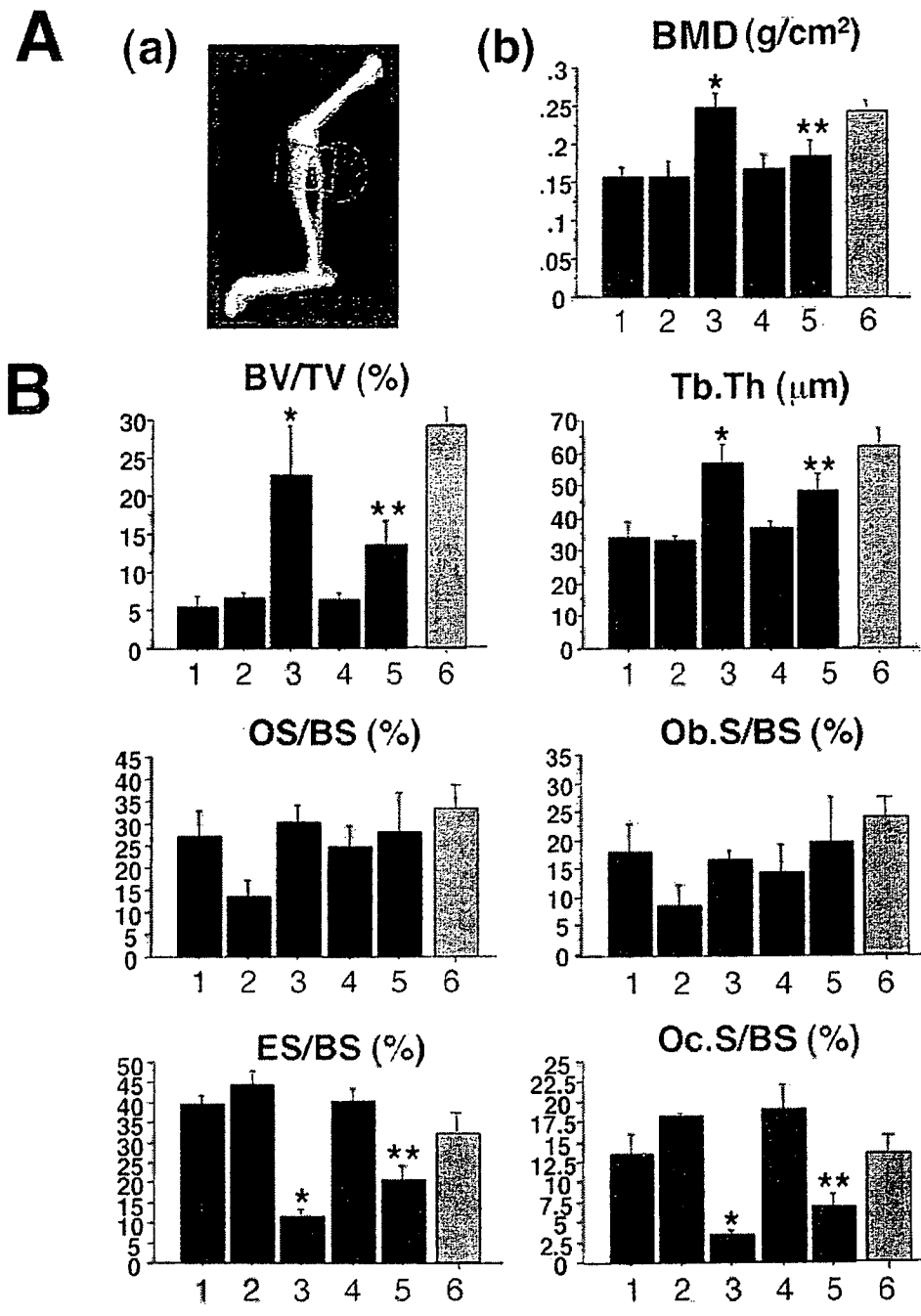

Fig. 3A,B. Effect on the bone mineral density (*BMD*) and histomorphometric parameters. **A** BMD analysis. (**a**) The BMD of the proximal one-third of tibia was measured by a bone densitometer using special software provided by the manufacturer. The region-of-interest tool was employed to define the proximal tibia and to eliminate the fibula from the scans. (**b**) Data are shown as the mean ± SD for five rats in each experimental group: *1*, untreated CIA group; *2*, indomethacin group; *3*, dexamethasone group; *4*, cele.5 group; *5*, cele.50 group; *6*, normal control group. $^{*}P < 0.01$, $^{**}P < 0.05$ for the untreated CIA group vs the dexamethasone and cele.50 groups, respectively (ANOVA). **B** Histomorphometric analysis. *1*, untreated CIA group; *2*, indomethacin group; *3*, dexamethasone group; *4*, cele.5 group; *5*, cele.50 group; *6*, normal control group. Both BV/TV and Tb.Th were significantly preserved in the cele.50 group (*5*) and the dexamethasone group (*3*). $^{*}P < 0.01$, $^{**}P < 0.05$ for the untreated CIA group vs the dexamethasone group and cele.50 group, respectively (ANOVA). *BV/TV*, trabecular bone volume; *Tb.Th*, trabecular thickness; *OS/BS*, osteoid surface relative to bone surface; *Ob.S/BS*, osteoblast surface relative to bone surface; *ES/BS*, eroded surface quantified relative to the bone surface; *Oc.S/BS*, osteoclast surface quantified relative to the bone surface

vented the growth plate destruction that usually occurs in CIA. In contrast, low-dose celecoxib (5 mg/kg per day) did not demonstrate a preventive effect on juxta-articular osteopenia or growth plate destruction, although it still reduced inflammation. These findings suggest that celecoxib may have different actions at high doses from those seen at low doses. The low dose of celecoxib used in this study is similar to the clinical dosage for RA patients and there have been no previous reports about the improvement of juxta-articular osteopenia and growth plate destruction by celecoxib in either the experimental or clinical setting. Therefore, further investigations will be necessary to better define this anti-osteoporotic effect of celecoxib, including studies on juxta-articular osteopenia and growth plate destruction in patients with RA and JIA.

Animals with CIA, including rats and mice, are commonly used to investigate the pathology of inflammatory arthritides such as RA or to confirm the effects of anti-inflammatory drugs. Previously, Bogoch et al.[19] reported the occurrence of juxta-articular bone loss in rabbits with experimental inflammatory arthritis. Hanyu et al.[25] concluded that the cause of juxta-articular osteopenia in CIA rats was a significant increase of osteoclasts along with a decrease in the rate of bone formation based on their histomorphomet-

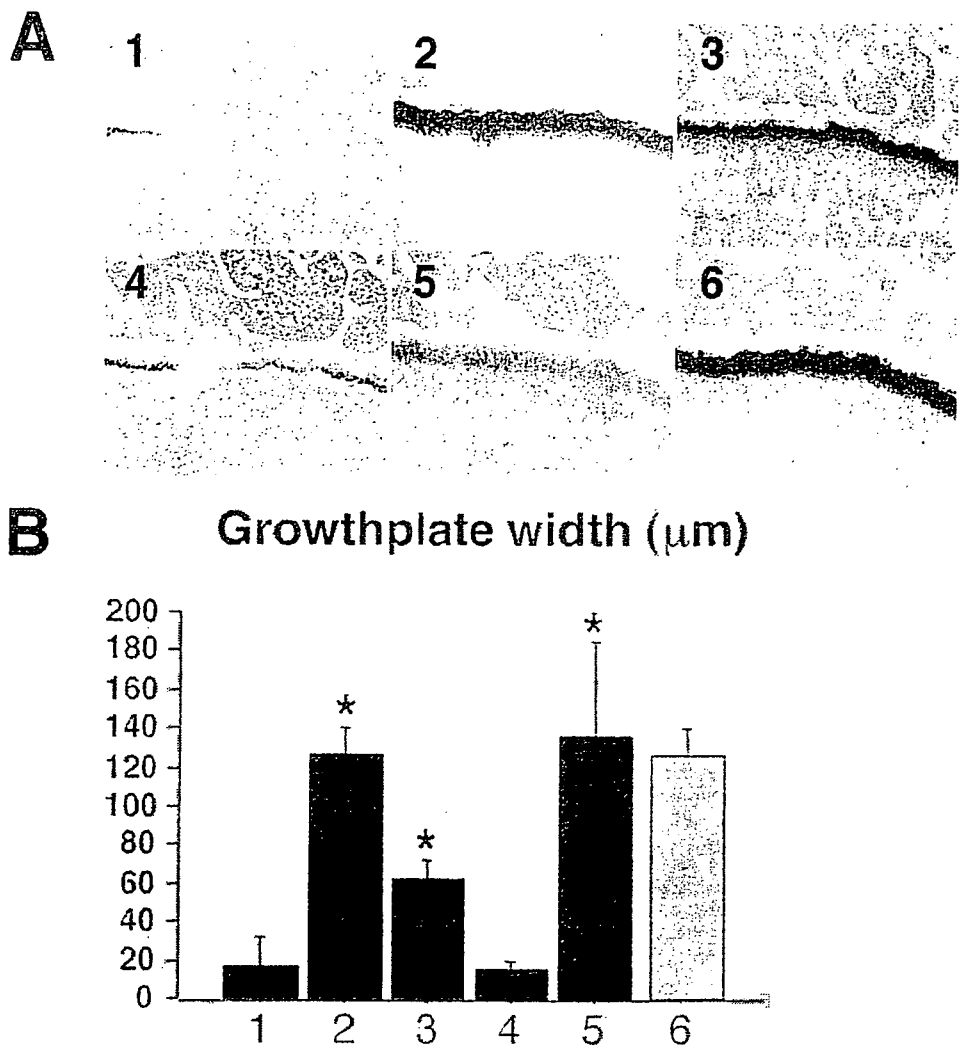

Fig. 4A,B. Effect on growth plate destruction. **A** Histological findings in the *1*, untreated CIA group; *2*, indomethacin group; *3*, dexamethasone group; *4*, cele.5 group; *5*, cele.50 group; *6*, normal control group. **B** Growth plate width. Measurement of the proximal tibial growth plate showed that it was significantly wider in the indomethacin, dexamethasone, and cele.50 groups than in the untreated CIA group or cele.5 group. Both indomethacin and high-dose celecoxib were more effective than dexamethasone. $^*P < 0.01$ for untreated CIA group vs the indomethacin, dexamethasone, and cele.50 groups (ANOVA)

ric analysis. Juxta-articular osteopenia is a typical finding in RA patients, and osteoclasts are often observed in the juxta-articular region on histological examination.[1,26–30] Accordingly, osteoclasts are thought to play an important role in the occurrence of juxta-articular osteopenia in patients with RA, especially when there is rapid bone erosion. Hanyu et al.[25] also reported a decrease in the rate of bone formation in CIA rats. Our histomorphometric analysis demonstrated that the protective effect of high-dose celecoxib against bone loss in CIA rats was associated with a significant decrease of bone resorption by osteoclasts. However, high-dose celecoxib could not ameliorate the decrease of bone formation parameters in CIA, indicating that decreased bone resorption by osteoclasts may be the major action by which high-dose celecoxib prevents bone loss.

Recently, high-dose celecoxib was reported to induce apoptosis of cancer cells, stromal cells, and rheumatoid synovial fibroblasts, although low doses do not have an apoptogenic effect.[31–35] This was an unexpected finding for a COX-2 inhibitor, and it seems to be a specific action of celecoxib alone.[31–35] Accordingly, osteoclastogenesis in the juxta-articular region might have been suppressed by decreased RANKL expression on fibroblasts or stromal cells, which is essential for osteoclastogenesis to occur,[26–30] through both the inhibition of PG production and an apoptotic effect on these cells. Therefore, juxta-articular osteopenia may have been improved by a decrease of osteoclasts as our bone histomorphometric analysis showed. Furthermore, our data suggest that high-dose celecoxib may not only prevent inflammation but also juxta-articular osteopenia in patients with RA.

Although low-dose celecoxib and indomethacin had an excellent anti-inflammatory effect, neither agent improved juxta-articular osteopenia in CIA rats. Thus, the low dose of celecoxib and the dose of indomethacin that we tested (a common clinical dose) may have been insufficient to inhibit osteoclastogenesis in CIA rats. It has already been reported that methotrexate and dexamethasone can inhibit joint destruction in rats with arthritis,[36–38] but there have been no studies showing that NSAIDs including COX-2 inhibitors could prevent juxta-articular osteopenia. It may be necessary to suppress disease activity more strongly to prevent

juxta-articular osteopenia in RA patients. The present results also imply that the usual dose of celecoxib may be too low to prevent juxta-articular osteopenia in RA patients, although it is effective against inflammation. Because high-dose celecoxib could reduce juxta-articular osteopenia in CIA rats, high-dose therapy may be a possible new modality to prevent juxta-articular osteopenia in patients with RA.

In the present study, we demonstrated that indomethacin and high-dose celecoxib almost completely prevented early growth plate closure in CIA rats, while dexamethasone partially prevented growth plate destruction. We previously reported[20] that early closure of epiphyseal growth plates led to poor development of the long bones in CIA rats and showed that overexpression of matrix metalloproteinase-3 (MMP-3), which may be involved in proteoglycan degradation, and vascular endothelial growth factor (VEGF), which is associated with cartilage ossification and angiogenesis, might play a role. Therefore, VEGF may be involved in causing an increase of osteoclasts/chondroclasts, which results in destruction of the growth plate. Our histomorphometric analysis demonstrated a decrease of osteoclasts in the dexamethasone group and the cele.50 group, findings that may explain one of the mechanisms preventing growth plate destruction. Abdelrahim and Safe[39] reported that COX-2 inhibitors decrease VEGF expression by colon cancer cells, while Sanchez et al.[40] reported that NSAIDs (including COX-2 inhibitors) did not alter MMP-3 production by cultured human chondrocytes. These finding may also help to explain the mechanism by which celecoxib prevented growth plate destruction in CIA rats. On the other hand, although dexamethasone completely abolished paw swelling and juxta-articular osteopenia, it only had a limited preventive effect on growth plate destruction. It was recently reported that dexamethasone can damage the growth plate in rats by causing apoptosis of growth plate chondrocytes.[41] Therefore, the dose of dexamethasone that suppresses arthritis may concurrently have an adverse influence on the growth plate in rats. A decrease of BMD is common in children and adolescents with JIA, resulting in reduced bone mass and a higher risk of osteoporosis.[42] Taking this point into consideration, it is not only important to reduce inflammation but also bone loss in patients with JIA. High-dose celecoxib may be a new candidate to prevent juxta-articular osteopenia in patients with JIA as well as RA, while also maintaining growth plate integrity in JIA patients whose growth plates are still open.

In conclusion, our findings suggested that a selective COX-2 inhibitor, celecoxib, is not only effective against inflammation, but also prevents juxta-articular osteopenia adjacent to inflamed joints in rats with CIA. Moreover, this drug prevents destruction of the growth plates adjacent to inflamed joints, which occurs in JIA and leads to premature growth plate closure with resultant epiphyseal deformity.

Acknowledgments The authors thank Akemi Ito for performing the histomorphometrical analysis. This work was supported in part by a grant-in-aid from the Health Science Research Grant from the Ministry of Health and Welfare of Japan.

References

1. Gravallese EM, Harada Y, Wang JT, Gorn AH, Thornhill TS, Goldring SR. Identification of cell types responsible for bone resorption in rheumatoid arthritis and juvenile rheumatoid arthritis. Am J Pathol 1998;152:943–51.
2. Tak PP, Bresnihan B. The pathogenesis and prevention of joint damage in rheumatoid arthritis: advances from synovial biopsy and tissue analysis. Arthritis Rheum 2000;43:2619–33.
3. Krane SM. Mechanism of tissue destruction in rheumatoid arthritis. Arthritis and allied conditions. 12th ed. Malvern, PA: Lea & Febiger; 1993.
4. Simon S, Whiffen J, Shapiro F. Leg-length discrepancies in monoarticular and pauciarticular juvenile rheumatoid arthritis. J Bone Joint Surg (A) 1981;63(2):209–15.
5. Meade EA, Smith WL, DeWitt DL. Differential inhibition of prostaglandin endoperoxide synthase (cyclooxygenase) isozymes by aspirin and other non-steroidal anti-inflammatory drugs. J Biol Chem 1993;268(9):6610–4.
6. O'Neill GP, Mancini JA, Kargman S, Yergey J, Kwan MY, Falgueyret JP, et al. Overexpression of human prostaglandin G/H synthase-1 and -2 by recombinant vaccinia virus: inhibition by nonsteroidal anti-inflammatory drugs and biosynthesis of 15-hydroxyeicosatetraenoic acid. Mol Pharmacol 1994;45(2):245–54.
7. Bombardieri S, Cattani P, Ciabattoni G, Di Munno O, Pasero G, Patrono C, et al. The synovial prostaglandin system in chronic inflammatory arthritis: differential effects of steroidal and non-steroidal anti-inflammatory drugs. Br J Pharmacol 1981;73(4):893–901.
8. Davies P, Bailey PJ, Goldenberg MM, Ford-Hutchinson AW. The role of arachidonic acid oxygenation products in pain and inflammation. Annu Rev Immunol 1984;2:335–57.
9. O'Neill GP, Ford-Hutchinson AW. Expression of mRNA for cyclooxygenase-1 and cyclooxygenase-2 in human tissues. FEBS Lett 1993;330(2):156–60.
10. Crofford LJ. COX-2 in synovial tissues. Osteoarthritis Cartilage 1999;7(4):406–8.
11. Okada Y, Lorenzo JA, Freeman AM, Tomita M, Morham SG, Raisz LG, et al. Prostaglandin G/H synthase-2 is required for maximal formation of osteoclast-like cells in culture. J Clin Invest 2000;105(6):823–32.
12. Okada Y, Pilbeam C, Raisz L, Tanaka Y. Role of cyclooxygenase-2 in bone resorption. J UOEH 2003;25(2):185–95.
13. Yasuda H, Shima N, Nakagawa N, Yamaguchi K, Kinosaki M, Mochizuki S, et al. Osteoclast differentiation factor is a ligand for osteoprotegerin/osteoclastogenesis-inhibitory factor and is identical to TRANCE/RANKL. Proc Natl Acad Sci USA 1998;95(7):3597–602.
14. Ilowite NT. Current treatment of juvenile rheumatoid arthritis. Pediatrics 2002;109(1):109–15.
15. Kawaguchi H, Chikazu D, Nakamura K, Kumegawa M, Hakeda Y. Direct and indirect actions of fibroblast growth factor 2 on osteoclastic bone resorption in cultures. J Bone Miner Res 2000;15(3):466–73.
16. Igarashi K, Woo JT, Stern PH. Effects of a selective cyclooxygenase-2 inhibitor, celecoxib, on bone resorption and osteoclastogenesis in vitro. Biochem Pharmacol 2002;63(3):523–32.
17. Katagiri M, Ogasawara T, Hoshi K, Chikazu D, Kimoto A, Noguchi M, et al. Suppression of adjuvant-induced arthritic bone destruction by cyclooxygenase-2 selective agents with and without inhibitory potency against carbonic anhydrase II. J Bone Miner Res 2006;21(2):219–27.
18. Mastbergen SC, Lafeber FP, Bijlsma JW. Selective COX-2 inhibition prevents proinflammatory cytokine-induced cartilage damage. Rheumatology (Oxford) 2002;41(7):801–8.
19. Bogoch E, Gschwend N, Bogoch B, Rahn B, Perren S. Juxta-articular bone loss in experimental inflammatory arthritis. J Orthop Res 1988;6(5):648–56.
20. Takahi K, Hashimoto J, Hayashida K, Shi K, Takano H, Tsuboi H, et al. Early closure of growth plate causes poor growth of long bones in collagen-induced arthritis rats. J Musculoskelet Neuronal Interact 2002;2(4):344–51.
21. Tomita T, Takeuchi E, Tomita N, Morishita R, Kaneko M, Yamamoto K, et al. Suppressed severity of collagen-induced ar-

thritis by in vivo transfection of nuclear factor κB decoy oligodeoxynucleotides as a gene therapy. Arthritis Rheum 1999;42(12): 2532–42.
22. Nagy TR, Prince CW, Li J. Validation of peripheral dual-energy X-ray absorptiometry for the measurement of bone mineral in intact and excised long bones of rats. J Bone Miner Res 2001;16(9): 1682–7.
23. Nishida S, Yamaguchi A, Tanizawa T, Endo N, Mashiba T, Uchiyama Y, et al. Increased bone formation by intermittent parathyroid hormone administration is due to the stimulation of proliferation and differentiation of osteoprogenitor cells in bone marrow. Bone 1994;15(6):717–23.
24. Parfitt AM, Drezner MK, Glorieux FH, Kanis JA, Malluche H, Meunier PJ, et al. Bone histomorphometry: standardization of nomenclature, symbols, and units. Report of the ASBMR Histomorphometry Nomenclature Committee. J Bone Miner Res 1987; 2(6):595–610.
25. Hanyu T, Chotanaphuti T, Arai K, Tanaka T, Takahashi HE. Histomorphometric assessment of bone changes in rats with type II collagen-induced arthritis. Bone 1999;24(5):485–90.
26. Gravallese EM, Manning C, Tsay A, Naito A, Pan C, Amento E, et al. Synovial tissue in rheumatoid arthritis is a source of osteoclast differentiation factor. Arthritis Rheum 2000;43(2):250–8.
27. Takayanagi H, Iizuka H, Juji T, Nakagawa T, Yamamoto A, Miyazaki T, et al. Involvement of receptor activator of nuclear factor kappaB ligand/osteoclast differentiation factor in osteoclastogenesis from synoviocytes in rheumatoid arthritis. Arthritis Rheum 2000;43(2):259–69.
28. Shigeyama Y, Pap T, Kunzler P, Simmen BR, Gay RE, Gay S. Expression of osteoclast differentiation factor in rheumatoid arthritis. Arthritis Rheum 2000;43(11):2523–30.
29. Hirayama T, Danks L, Sabokbar A, Athanasou NA. Osteoclast formation and activity in the pathogenesis of osteoporosis in rheumatoid arthritis. Rheumatology (Oxford) 2002;41(11):1232–39.
30. Udagawa N, Kotake S, Kamatani N, Takahashi N, Suda T. The molecular mechanism of osteoclastogenesis in rheumatoid arthritis. Arthritis Res 2002;4(5):281–9.
31. Hsu AL, Ching TT, Wang DS, Song X, Rangnekar VM, Chen CS. The cyclooxygenase-2 inhibitor celecoxib induces apoptosis by blocking Akt activation in human prostate cancer cells independently of Bcl-2. J Biol Chem 2000;275(15):11397–403.
32. Grosch S, Tegeder I, Niederberger E, Brautigam L, Geisslinger G. COX-2 independent induction of cell cycle arrest and apoptosis in colon cancer cells by the selective COX-2 inhibitor celecoxib. FASEB J 2001;15(14):2742–4.
33. Leahy KM, Ornberg RL, Wang Y, Zweifel BS, Koki AT, Masferrer JL. Cyclooxygenase-2 inhibition by celecoxib reduces proliferation and induces apoptosis in angiogenic endothelial cells in vivo. Cancer Res 2002;62(3):625–31.
34. Kusunoki N, Yamazaki R, Kawai S. Induction of apoptosis in rheumatoid synovial fibroblasts by celecoxib, but not by other selective cyclooxygenase 2 inhibitors. Arthritis Rheum 2002;46(12): 3159–67.
35. Kusunoki N, Ito T, Sakurai N, Suguro T, Handa H, Kawai S. A novel celecoxib derivative potently induces apoptosis of human synovial fibroblasts. J Pharmacol Exp Ther 2005;314(2):796–803.
36. Kawai S, Nagai K, Nishida S, Sakyo K, Murai E, Mizushima Y. Low-dose pulse methotrexate inhibits articular destruction of adjuvant arthritis in rats. J Pharm Pharmacol 1997;49(2):213–5.
37. Segawa Y, Yamaura M, Aota S, Omata T, Tuzuike N, Itokazu Y, et al. Methotrexate maintains bone mass by preventing both a decrease in bone formation and an increase in bone resorption in adjuvant-induced arthritic rats. Bone 1997;20(5):457–64.
38. Takagi T, Tsao PW, Totsuka R, Suzuki T, Murata T, Takata I. Dexamethasone prevents the decrease of bone mineral density in type II collagen-induced rat arthritis model. Jpn J Pharmacol 1998;78(2):225–8.
39. Abdelrahim M, Safe S. Cyclooxygenase-2 inhibitors decrease vascular endothelial growth factor expression in colon cancer cells by enhanced degradation of Sp1 and Sp4 proteins. Mol Pharmacol 2005;68(2):317–29.
40. Sanchez C, Mateus MM, Defresne MP, Crielaard JM, Reginster JY, Henrotin YE. R Metabolism of human articular chondrocytes cultured in alginate beads. Longterm effects of interleukin 1beta and nonsteroidal anti-inflammatory drugs. J Rheumatol 2002;29(4): 772–82.
41. Chrysis D, Ritzen EM, Savendahl L. Growth retardation induced by dexamethasone is associated with increased apoptosis of the growth plate chondrocytes. J Endocrinol 2003;176(3):331–7.
42. McDonagh JE. Osteoporosis in juvenile idiopathic arthritis (Review). Curr Opin Rheumatol 2001;13(5):399–404.

The mode of destruction in shoulders with rheumatoid arthritis based on radiographic findings

Hiroyuki Tanaka, MD,[a] Kazuomi Sugamoto, MD, PhD,[b] Wataru Sahara, MD,[b] Takeshi Ono, MD,[b] Tetsuya Tomita, MD, PhD,[b] Jun Hashimoto, MD, PhD,[b] and Hideki Yoshikawa, MD, PhD,[b] *Osaka, Japan*

The objective of the present study was to elucidate the mode of rheumatoid arthritis shoulder destruction. The study included 402 shoulders from 201 patients with rheumatoid arthritis. Plain radiographic findings were used to assess and statistically analyze the severity of the glenohumeral joint destruction (GHD) and greater tuberosity destruction (GTD).For both GHD and GTD scores, a statistically significant correlation was found between the left and right sides and also between the GHD and GTD scores within the same shoulder. However, 97 shoulders of 67 patients showed a heterogeneous pattern. An interesting finding was that no patients showed a combination of the GHD type plus the GTD type. Shoulders with rheumatoid arthritis showed statistically significant symmetry and uniform destruction. Even if they showed heterogeneous destruction, there were no cases of a different pattern of heterogeneity on the opposite side. The mode of destruction was not always definite, however. (J Shoulder Elbow Surg 2007;16:539-543.)

Joint destruction due to rheumatoid arthritis (RA) is well documented, and the shoulder is one of the joints most often affected.[3,11,12,13,18,19] Joint destruction caused by RA is generally bilateral and symmetrical[13,19,8,4,21]; however, we have demonstrated that joint destruction is unilateral in some patients, with a marked left versus right difference in the severity of destruction. In addition, the homogeneity of destruction within the same joint can vary.

We focused on 2 important areas of the proximal humerus, the joint surface and the greater tuberosity, because destruction of these areas seemed to be related to clinical symptoms such as joint congruity or rotator cuff function. We also wanted to determine the frequency and tendency toward heterogeneous or asymmetric destruction of the RA shoulder. We, therefore, initiated a large-scale radiographic study with the objective of elucidating the mode of RA shoulder joint bone destruction.

From the [a]Department of Orthopedics, Kawasaki Hospital; and [b]Department of Orthopedics, Osaka University Hospital.

Reprint requests: Hiroyuki Tanaka, MD, Department of Orthopedics, Kawasaki Hospital, Sawa 485-1-502, Kaizuka-shi, Osaka, Japan 597-0062 (E-mail: *hiro145@rinku.zaq.ne.jp*).

1058-2746/2007/$32.00
doi:10.1016/j.jse.2006.11.011

MATERIALS AND METHODS

Patients

Between 2001 and 2003, 233 patients visited the Department of Orthopaedics at the Osaka University Hospital. They satisfied the diagnostic criteria established by the American College of Rheumatology[1] and underwent bilateral plain radiography. Of these 233 patients, 32 were excluded: 5 patients who had undergone joint replacement in both shoulders, 7 who had undergone joint replacement in 1 shoulder, and 20 for whom definitive radiographic findings could not be obtained for 1 or both sides. Consequently, 402 shoulders from 201 patients (26 men, 175 women) were included in this study. Their average age was 57.0 years (range, 23-84 years).

Plain radiography

Joint destruction was assessed from anteroposterior radiographs of the left and right shoulder joints taken at the final examination. The radiographs were taken by placing each patient in the supine position, tilting the contralateral side 20° relative to the direction of the x-ray tube, positioning the upper arm into lateral rotation with the palm facing upward, and then taking radiographs perpendicular to the glenohumeral joint.

Assessment of plain radiographs

Larsen's classification system[10] was used to classify glenohumeral joint destruction (GHD) into 6 grades (grades 0-5). The severity of greater tuberosity destruction (GTD) (bone erosion and radiolucency) was assessed by the depth from the top of the greater tuberosity to the bottom of the osseous lesion and was classified into 3 grades: as mild (depth, <5 mm), moderate (:depth, 5-10 mm); and severe (depth, ≥10 mm; see Figure 1).

Pattern of destruction

We classified the pattern of destruction within a shoulder into 4 types at the point of the most severely affected area as follows:

1. GHD type (heterogeneous osseous lesion in a severely eroded glenohumeral joint): GHD grade 4 or

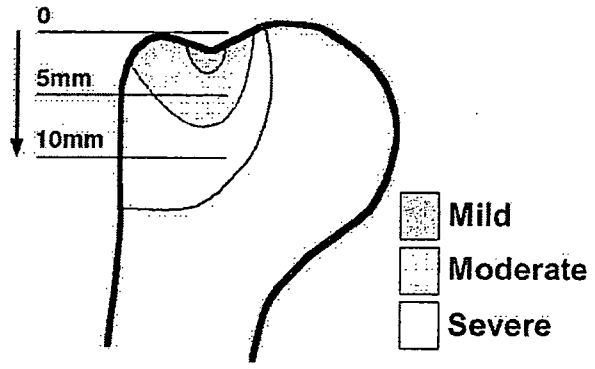

Figure 1 The destruction of the greater tuberosity was assessed by its depth from the top of the greater tuberosity to the bottom of the osseous lesion. The depth was classified into three grades: mild *(dark gray)* was less than 5 mm; moderate *(medium gray)* was between 5 and 10 mm; and severe *(light gray)* was 10 mm or more.

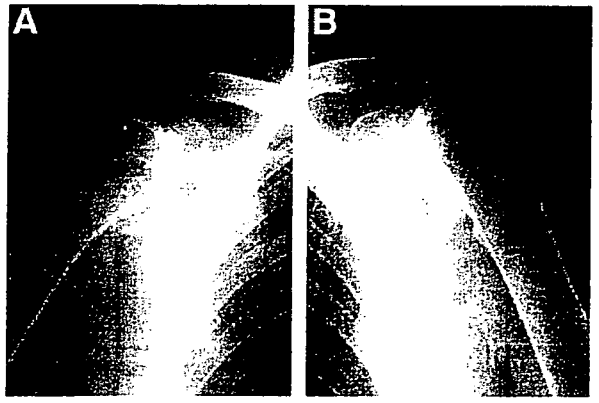

Figure 2 A and B, Radiographs of the rheumatoid shoulders of a 61-year-old woman show bilateral grade 5 glenohumeral joint destruction (GHD), and a mild grade of greater tuberosity destruction. Both shoulders showed extensive erosive destruction of articular surface, both osseous lesions of the greater tuberosity were mild. The destruction pattern was symmetric GHD type. The destruction was symmetrical.

more, GTD grade mild or moderate (see Figures 2A and B, 3A)
2. GTD type (heterogeneous osseous lesion in a severely eroded greater tuberosity): GHD grade 3 or less, GTD grade severe (Figure 4B)
3. Uniformly mild: GHD grade 3 or less, GTD grade mild or moderate (Figures 3B and 4A)
4. Uniformly severe: GHD grade 4 or more, GTD grade severe

We classified the GHD and GTD types as heterogeneous destruction.

Data analysis

Paired comparisons between men and women were performed with the Mann-Whitney *U* test for GTD and GHD scores. The correlation between age and osseous destruction, between individual left and right sides, and between the GHD and GTD scores within the same shoulder were made with Spearman rank correlation coefficients.

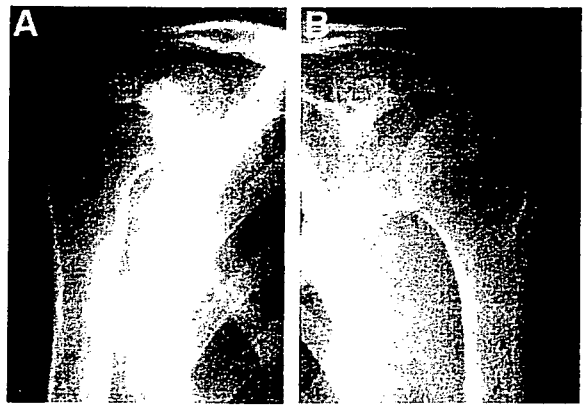

Figure 3 Radiographs of the rheumatoid shoulders of a 62-year-old woman. **A,** The right shoulder was at grade 5, and had mild GTD. It showed extensive osseous lesion in the articular surface, but there was little osseous lesion in the greater tuberosity. The destruction pattern was GHD, uniformly mild type. The destruction was asymmetrical. **B,** The left shoulder showed no pronounced lesion and was at glenohumeral joint destruction (GHD) grade 1. It had a mild grade of greater tuberosity destruction (GTD).

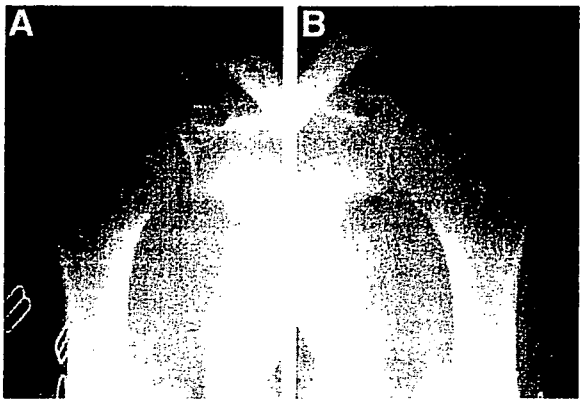

Figure 4 Radiographs of the rheumatoid shoulders of a 52-year-old woman. **A,** The right shoulder was at glenohumeral joint destruction (GHD) grade 1 and had a mild grade of greater tuberosity destruction (GTD). It showed no pronounced osseous lesion. **B,** The left shoulder was at GHD grade 2 and a severe grade of GTD. It showed an extensive osseous lesion in the greater tuberosity, but the original articular surface had not yet disappeared. The destruction pattern was uniformly mild/GTD type. The destruction was asymmetrical.

RESULTS

Classification of glenohumeral destruction and greater tuberosity destruction

Glenohumeral destruction. According to a. Larsen's classification system, the severity of GHD was classified

Table I Radiographic assessment by Larsen method of the glenohumeral joints in 201 patients with rheumatoid arthritis*

	Right GHD grade						
	0	1	2	3	4	5	Total
Left GHD grade (No. of joints)							
0	2	0	0	0	0	0	2
1	0	30	17	0	1	3	51
2	0	10	47	12	1	3	73
3	0	0	9	9	4	1	23
4	0	0	3	1	5	4	13
5	0	3	2	1	5	28	39
Total	2	43	78	23	16	39	201

GHD, Glenohumeral joint destruction.
*The number of the left GHD grade for each right GHD grade is presented. The grade of GHD between individual left and right sides is significantly correlated ($r = 0.69$, $P < .001$).

Table II Radiographic assessment of the greater tuberosity destruction in 201 patients with rheumatoid arthritis*

	Right GTD grade			
	Mild	Moderate	Severe	Total
Left GTD grade (No. of joints)				
Mild	48	17	4	69
Moderate	9	75	14	98
Severe	2	8	24	34
Total	59	100	42	201

GTD, Greater tuberosity destruction.
*The number of the left GTD grade for each right GTD grade is presented. The grade of the GTD between individual left and right sides is significantly correlated ($r = 0.65$, $P < .001$).

into 6 grades: grade 0 in 4 joints (1.0%), grade 1 in 94 joints (23.3%), grade 2 in 151 joints (37.6%), grade 3 in 46 joints (11.4%), grade 4 in 29 joints (7.2%), and grade 5 in 78 joints (19.4%). Thus, 107 (26.7%) of 402 joints had a grade of 4 or more (Table I).

Greater tuberosity destruction. As described earlier, the severity of the GTD was classified into 3 grades: mild in 128 shoulders (31.8%), moderate in 198 shoulders (49.3%), and severe in 76 shoulders (18.9%; Table II).

Statistical analysis

A comparison of gender and GHD or GTD scores found no significant difference between men and women in GHD ($P = .26$) and GTD scores ($P = .67$).

There was no correlation between age and the GHD ($r = 0.11$; $P = .03$) or GTD ($r = -0.09$; $P = .35$) scores. Significant correlations were found between the individual left and right sides (Tables I and II) for both. GHD ($r = 0.69$, $P < .001$) and; GTD ($r = 0.65$, $P < .001$) and between GHD and GTD ($r = 0.58$, $P < .001$) within the same shoulder (Table III).

Table III The number of the greater tuberosity destruction grade is presented for each glenohumeral joint destruction grade in 402 shoulders from 201 patients*

	GHD grade						
	0	1	2	3	4	5	Total
GTD grade (No. of joints)							
Mild	4	63	54	6	0	1	128
Moderate	0	31	82	22	16	47	198
Severe	0	0	15	18	13	30	76
Total	4	94	151	46	29	78	402

GTD, Greater tuberosity destruction; *GHD,* glenohumeral joint destruction.
*There was a significant correlation between the grade of GHD and GTD ($r = 0.58$, $P < .001$).

Table IV The pattern of the opposite side is presented in 67 patients with heterogeneity of destruction

	Pattern of opposite side			
	Uniformly mild*	Symmetric	Uniformly severe†	Total
GHD type	13	22	7	42
GTD type	14	8	3	25
Total	27	30	10	67

GHD, Glenohumeral joint destruction; GTD, greater tuberosity destruction.
*GHD grade ≤3, GTD grade is severe.
†GHD grade ≥4, GTD grade mild or moderate. No case showed asymmetric heterogeneous pattern.

Heterogeneous destruction within a shoulder

We showed that there was a significant correlation between the GHD and GTD scores within the same shoulder. However, we investigated 97 shoulders (24.1%) from 67 patients who showed a heterogeneous pattern within their shoulders of the GHD type (64 shoulders in 42 patients) and GTD type (33 shoulders in 25 patients).

We then assessed the pattern of destruction on the opposite side for these patients (see Table IV). In the GHD type, 22 (52.4%) of 42 patients showed a symmetrical pattern. In the same manner, in the GTD type, 8 (32.0%) of 25 patients showed a symmetrical pattern. No patients presented with heterogeneous patterns in which there was a combination of the GHD type and the GTD type.

DISCUSSION

In general, joint destruction caused by RA is bilateral and symmetrical.[4,8,13,19,21] One study showed that the left-right symmetry of the severity of joint destruction was especially pronounced in patients with severe RA.[13] Similarly, in the present study, there was a statistically significant correlation in the GHD and GTD scores between the left and right sides. In addition, a significant correlation was found between the GHD and GTD scores within the same shoulder.

Many studies[4,8,13,19,21] have compared the presence of joint destruction between left and right shoulders but did not compare the severity of destruction between the sides or between different areas within the same shoulder. Like previous reports on shoulder joint destruction, the present study involved many patients. Many patients were mildly affected, however, and that may have reduced the probability that we could detect statistically significant differences between individual sides or the mode of destruction within a joint.

We believe that the joint surface and the greater tuberosity are clinically important parts of the proximal humerus because of their role in joint congruity and rotator cuff function, respectively. Lehtinen et al[13] confirmed radiographically that the mildest sign in the rheumatoid shoulder is marginal erosion on the superolateral articular margin of the humerus. We therefore assessed the presence of osseous lesions of these 2 areas.

The present study assessed,the severity of GHD and GTD. There were correlations in the GHD and GTD scores between the same sides (Tables I and II) and between the GHD and GTD scores within the same shoulder (Table III). With respect to GHD, only 18 patients (9.0%) showed a clear difference between their left and right sides (>2 grades separation; Table I). With respect to GTD, only 6 patients (3.0%) showed a clear difference between their left and right sides (>2 grades separation; Table II). Conversely, within the same shoulder, 97 shoulders from 67 patients that showed a heterogeneous pattern: 64 shoulders from 42 patients for the GHD type, and 33 shoulders from 25 patients for the GTD type. In the GHD type, 22 (52.4%) of 42 patients showed a symmetrical pattern. Similarly, in the GTD type, 8 (32.0%) of 25 patients showed a symmetrical pattern. An interesting finding was that no patients showed a combination of the GHD type plus the GTD type (Table IV).

This suggests that most patients showed uniform and symmetrical destruction. Even if the cases showed heterogeneous destruction within the same shoulder, the opposite side always showed a symmetrical, heterogeneous pattern or uniform destruction. This did not seem to be a random occurrence.

We considered 2 factors that might cause this variety of destruction. First, absorption of the cartilage and bone as a result of the actions of cytokines released from the synovial tissue or direct destruction of the marginal bone may have resulted in these differing patterns. The second factor was the effects from anatomic and mechanical factors. Some studies have shown that mechanical stress can affect shoulder destruction. Other studies have found that hand dominance has no effect on the severity of joint destruction, suggesting that mechanical stress has little effect.[11-14] Because the shoulder joint is not a weight-bearing joint, mechanical stress may have a lesser effect than for weight-bearing joints such as the hip or knee. However, we could not generate a reliable hypothesis in this study to explain our results adequately. Ochi et al[18] reported that even in the same joint, the mechanism of destruction varies widely depending on the disease subset.

The condition of the bone and cartilage may affect the progression of bony destruction. This may be further affected by several factors, such as age, gender, medication, and the duration of the disease.[2,5-8,15,18,20] In this study, the severity of both GTD and GHD types did not seem to be affected significantly by gender or age in the statistical analysis. All of the present patients received some form of medication, but the drugs used and the time course of administration varied widely, making it difficult to assess the effects of drug-induced bone destruction. Furthermore, the disease durations were not assessed because of a lack of information from the patients. Regrettably, we could not assess other factors, such as laboratory data or the condition of the rotator cuff, joint cartilage, or bone marrow. Further studies are required to determine the mechanism of joint destruction using magnetic resonance imaging or more detailed clinical data.

In conclusion, shoulders with RA showed statistically significant symmetry and uniform destruction on plain radiographs. Even if the shoulders showed heterogeneous destruction, no patients presented with a different pattern of heterogeneity on the opposite side. The mode of destruction was not always definite, however: some subjects showed heterogeneous destruction within a joint, and a few showed unilateral destruction or a difference in the degree of destruction between left and right sides.[9,16,17]

REFERENCES

1. Arnett FC, Edworthy SM, Bloch DA, Mcshane DJ, Fries JF, Cooper NS, et al. The American Rheumatism Association 1987 revised criteria for the classification of rheumatoid arthritis. Arthritis Rheum 1988;31:315-24.
2. Brook A, Corbett M. Radiographic changes in early rheumatoid disease. Ann Rheum Dis 1997;36:71-3.

3. Crossan JF, Vallance R. The shoulder joint in rheumatoid arthritis. In: Bayley I, Kessel L, editors. Shoulder surgery. Berlin, Germany: Springer Verlag; 1982. p. 131-9.
4. Cuomo F, Greller MJ, Zuckerman JD. The rheumatoid shoulder. Rheum Dis Clin North Am 1998;24:67-82.
5. Dolan AL, Moniz C, Abraha H, Pitt P Does active treatment of rheumatoid arthritis limit disease-associated bone loss? Rheumatology 2002;41.1047-51
6. Firestein GS. Evolving concepts of rheumatoid arthritis. Nature 2003;423:356-61
7. Goldring SR. Bone and joint destruction in rheumatoid arthritis: what is really happening? J Rheumatol 2002;29:44-8.
8. Hirooka A, Wakitani S, Yoneda M, Ochi T. Shoulder destruction in rheumatoid arthritis: classification and prognostic sign in 83 patients followed 5-23 years. Acta Orthop Scand 1996;67:258-63.
9. Kirwan JR. The relationship between synovitis and erosions in rheumatoid arthritis. Br J Rheumatol 1997;36:225-8.
10. Larsen A, Dale K, Eek M. Radiographic evaluation of rheumatoid arthritis and related condition by standard reference film. Acta Radiol Diag 1997;18:481-91
11 Lehtinen JT, Belt EA, Kauppi MJ, Kaarela K, Kuusela PP, Kautiainen HJ, et al. Bone destruction, upward migration, and medialization of rheumatoid shoulder: a 15-year prospective follow-up study. Ann Rheum 2001;60:322-6.
12. Lehtinen JT, Belt EA, Lybeck CO, Kauppi MJ, Kaarela K, Kautinen HJ, et al. Subacromial space in the rheumatoid shoulder: a radiographic 15 year follow-up study of 148 shoulders. J Shoulder Elbow Surg 2000;9:183-7
13. Lehtinen JT, Kalevi K, Belt E, Kautiainen HJ, Kauppi MJ, Lehto MUK. Incidence of glenohumeral joint involvement in seropositive rheumatoid arthritis: a 15-year endpoint study. J Rheumatol 2000;27:347-50.
14. Lehtinen JT, Lehto MUK, Kaarela K, Kautiainen HJ, Belt EA, Kauppi MJ. Radiographic joint space in rheumatoid glenohumeral joints. A 15-year prospective follow-up study in 74 patients. J Rheumatol 2000;39:288-92.
15. McIlwain HH. Glucocorticoid-induced osteoporosis: pathogenesis, diagnosis, and management. Prev Med 2003;36:243-9.
16. Minaur NJ, Kounali D, Vedi S, Compston JE, Beresford JN, Bhalla K. Methotrexate in the treatment of rheumatoid arthritis: in vivo effects on bone mineral density. Rheumatology 2002;41:741-9.
17 Neer CS II. Reconstructive surgery and rehabilitation of the shoulder. In: Kelly WN, Harris ED Jr, Ruddy S, Sledge CB, editors. Textbook of rheumatology. Philadelphia, Pa: WB Saunders; 1985. p.1855-70.
18. Ochi T, Iwase R, Yonemasu K, Matsukawa M, Yoneda M, Yukioka M, et al. Natural course of joint destruction and fluctuation of serum C1q levels in patients with rheumatoid arthritis. Arthritis Rheum 1998;31:37-43.
19. Olofsson Y, Book C, Jacobsson LTH. Shoulder joint involvement in patients with newly diagnosed rheumatoid arthritis. Scand J Rheumatol 2003;32:25-32.
20. Solomon DH, Levin Elaine, Helfgott SM. Patterns of medication use before and after bone densitometry: Factors associated with appropriate treatment. J Rheumatol 2000;27·1496-500.
21 Tan AL, Tanner SF, Conaghan PG, Radjenovic A, O'Connor P, Brown AK, et al. Role of metacarpophalangeal joint anatomic factors in the distribution of synovitis and bone erosion in early rheumatoid arthritis. Arthritis Rheum 2003;48:1214-22.

In Vivo Three-Dimensional Skeletal Alignment Analysis of the Hindfoot Valgus Deformity in Patients with Rheumatoid Arthritis

Hongbo Liu,[1] Kazuomi Sugamoto,[2] Tomonobu Itohara,[3] Tetsuya Tomita,[3] Jun Hashimoto,[3] Hideki Yoshikawa[3]

[1]Department of Orthopaedic Surgery, Peking Union Medical College Hospital, Beijing, China

[2]Division of Robotic Therapy, Osaka University Graduate School of Medicine, Suita, Japan

[3]Department of Orthopaedic Surgery, Osaka University Graduate School of Medicine, Suita, Japan

Received 6 October 2005; accepted 20 July 2006

Published online 14 November 2006 in Wiley InterScience (www.interscience.wiley.com). DOI 10.1002/jor.20297

ABSTRACT: The purpose of this study was to analyze the skeletal alignment of the hindfoot valgus deformity in patients with rheumatoid arthritis using bone models reconstructed from three-dimensional computerized tomography data. Computed tomography was performed on 21 feet of patients with rheumatoid arthritis, and magnetic resonance imaging was taken of 10 normal feet of eight volunteers. An image processing system was used to create bone models and analyze the three-dimensional displacement of the calcaneus, talus, navicular, and cuboid bones. With a standard coordinate system in the distal tibia and a local coordinate system in each bone of the hindfoot, three rotational parameters and three translational parameters were used to evaluate the relative displacement. The talus showed plantar flexion. Both the calcaneus and navicular bones had valgus and lateral shift displacements. However, the cuboid had no displacement relative to the calcaneus, and the navicular showed no displacement relative to the cuboid. The calcaneus, navicular, and cuboid bones have the same pattern of deformity in patients with rheumatoid arthritis. This three-dimensional image-based technique successfully quantified the hindfoot valgus deformity resulting from rheumatoid arthritis and is beneficial for better understanding the deformity pathomechanism. © 2006 Orthopaedic Research Society. Published by Wiley Periodicals, Inc. J Orthop Res 25:330–339, 2007

Keywords: three-dimensional; skeletal alignment; hindfoot valgus deformity; rheumatoid arthritis

INTRODUCTION

Pes planovalgus deformity is a predominant hindfoot deformity in patients with rheumatoid arthritis (RA) with a prevalence of 46% to 64%.[1–5] Vahvanen reported that 87.4% of 292 surgically treated patients with RA showed pes planovalgus.[6] The clinical description of pes planovalgus deformity includes heel valgus, arch height loss, and forefoot abduction.[3–7] Although forefoot deformities are often the presenting complaints, as disease progresses, hindfoot involvement is a dominant, disabling defect that may need surgical stabilization and correction.[4,7,8]

Many clinicians and researchers have analyzed the deformity pattern using various methods, because analysis of the skeletal alignment of hindfoot valgus deformity in RA patients is crucial for understanding pathogenesis and the mechanism of the deformity and for preoperative planning. However, plain radiography lacks precision and accuracy, and images are difficult to obtain and measure in some RA patients.[7,9,10] Selzer and colleagues used two-dimensional (2D) coronal computed tomography (CT) to assess hindfoot valgus deformity.[8,11] This method did not allow a complete evaluation in three-dimensional (3D) ways and failed to reflect the deformities of the cuboid and navicular bones. Woodburn and colleagues used 3D imaging techniques to analyze the geometric architecture of the subtalar and midtarsal joints in cases of RA based on magnetic resonance imaging (MRI).[5] The twenty-four parameters they used are relatively complicated and can not provide clinicians with a good visualization of the deformity pattern.

In vivo 3D bony structural analysis of hindfoot valgus deformity in RA patients remains largely unexplored. A 3D imaging-based technique was developed by Osaka University to analyze bone

Correspondence to: Hongbo Liu (E-mail: liuhongbo1972@yahoo.com.cn)

This article includes Supplementary Material available via the Internet at http://www.interscience.wiley.com/jpages/0736-0266/suppmat.

morphology and joint kinematics. This system was successfully employed for motion analysis of the cervical spine[12,13] and wrist joint[14,15] and for ascertaining the pathological characteristics of clubfoot.[16] The purpose of this study was to analyze the pattern of RA hindfoot valgus deformity using this method.

MATERIALS AND METHODS

Fourteen patients with RA hindfoot valgus deformity were enrolled from the outpatient orthopedic department of Osaka University Afflicted Hospital. All patients met the American College of Rheumatology criteria (1995) for diagnosis of RA and Vahvanen's standard of valgus deformity (stages I–IV) in clinical manifestation and radiographic films.[6] X-ray films showed no distal tibofibular joint involvement. The mean age was 57 years (range, 39–71 years). The mean duration of disease was 11.7 years (range, 1–32 years). Eight healthy volunteers with no foot pain or medical history of foot disorders were recruited as controls. Their mean age was 27.8 years (range, 24–32 years). All participants gave written informed consent before the study began.

Analysis of RA hindfoot deformity was performed noninvasively, including data acquisition, segmentation, and 3D model reconstruction, and description of the deformity. Finally, the accuracy of this method was validated.

Data Acquisition

Computed tomography was performed on 21 feet of 14 patients with RA, and MRI was performed on 10 normal feet of 8 healthy volunteers who were considered as the control group. In a preliminary test, we found a significant loss of surface information from MRI data for feet from RA patients because of severe inflammation and bone erosion. The loss of surface information distorted the shape of the surface model and led to inaccurate analysis of the deformity pattern. As a sufficient number of RA patients who needed CT scans for preoperative planning were available in the outpatient orthopedic department, the 3D CT data were obtained for the patients with RA. To reduce radiation exposure, data were collected from healthy volunteers who underwent MRI.

CT from the distal third of the tibia and fibula to the end of the foot was performed for each patient using a clinical helical scanner (Light Speed Ultra 16; General Electric Company, Maukesha, WI) that produced 256 consecutive images with a section thickness of 0.625 mm. Scanning parameters were 120 kV and 120 to 240 mA. Total exposure time was about 24 min. MR images were taken using a 1.0 Tesla scanner (Sigma Horizontal LX ver. 9.1; General Electric Company, Milwaukee, WI). A TORSOPA coil was employed, and the 3D image was obtained using a 3D fast-GRASS (gradient recalled acquisition in the steady state) pulse sequence with a TR/TE ratio of recommended/minimum full and 1.5-mm slice thickness. The flip angle was 25°, and a 250-mm field of view (imaging matrix, 256 × 256) was used. Acquisition of each 3D volume imaging took about 3 min.

A custom nonmetallic orthosis was used to immobilize the ankle in a neutral position and to standardize the orientation of the foot relative to the ankle in the scanner. The device held the lower leg on a horizontal cushion and the foot against a vertical plate. With the lower leg secured, the foot position was adjusted until the neutral position of the ankle was achieved, then the foot was secured appropriately. If a neutral position could not be achieved due to an ankle deformity, the foot stayed in its natural unloaded position.

Segmentation and 3D Model Reconstruction

The contour of each hindfoot bone was semi-automatically extracted from 3D images by an intensity threshold technique using Virtual Place M.® software (AZE Ltd., Tokyo) developed in our laboratory. Surface models of the hindfoot and ankle joint of each participant were reconstructed from 3D image data using the marching cubes algorithm, in which areas with the same voxel values were surrounded by triangular patches.[17] Visualization was obtained by applying a modified version of Visualization Toolkit software (Kitware Inc., New York, NY). All left hindfoot 3D models were inverted for comparison with right hindfoot models.

Description of the Deformity

The tibia was used to set up a reference coordinate system, which was considered as the standard coordinate system (SCS). The purpose of using the SCS was to discern the displacements in the ankle, subtalar, and midtarsal joints relative to the tibia in RA patients. Displacement was defined as the change of a bone position from a normal position to a RA deformed position. The SCS was established from modification of the anatomical coordinate system of the tibia proposed by Cappozzo and colleagues.[18] The origin was located at the midpoint of the line joining the lateral malleoli (LM) and the medial malleoli (MM). The y-axis started from the origin and ran upward parallel to the long axis of the tibia. Thus, the y-axis and the line between the LM and MM formed a quasi-frontal plane. The x-axis was perpendicular to the plane defined by the y-axis and the line between the LM and MM, in the forward direction; the z-axis was orthogonal to the x- and y- axes in the lateral direction (Fig. 1). The long axis of the tibia was determined by the computer as passing through the center of gravity of the distal third of the tibia model and minimizing the moment of inertia. The LM and MM could be directly determined from the reconstructed bone models by identifying their tips.

To describe the displacement of the talus, calcaneus, navicular, and cuboid bones in the hindfoot, the position and orientation of each bone needed to be precisely define. A local coordinate system (LCS) was established for each of the four hindfoot bones. The establishment of

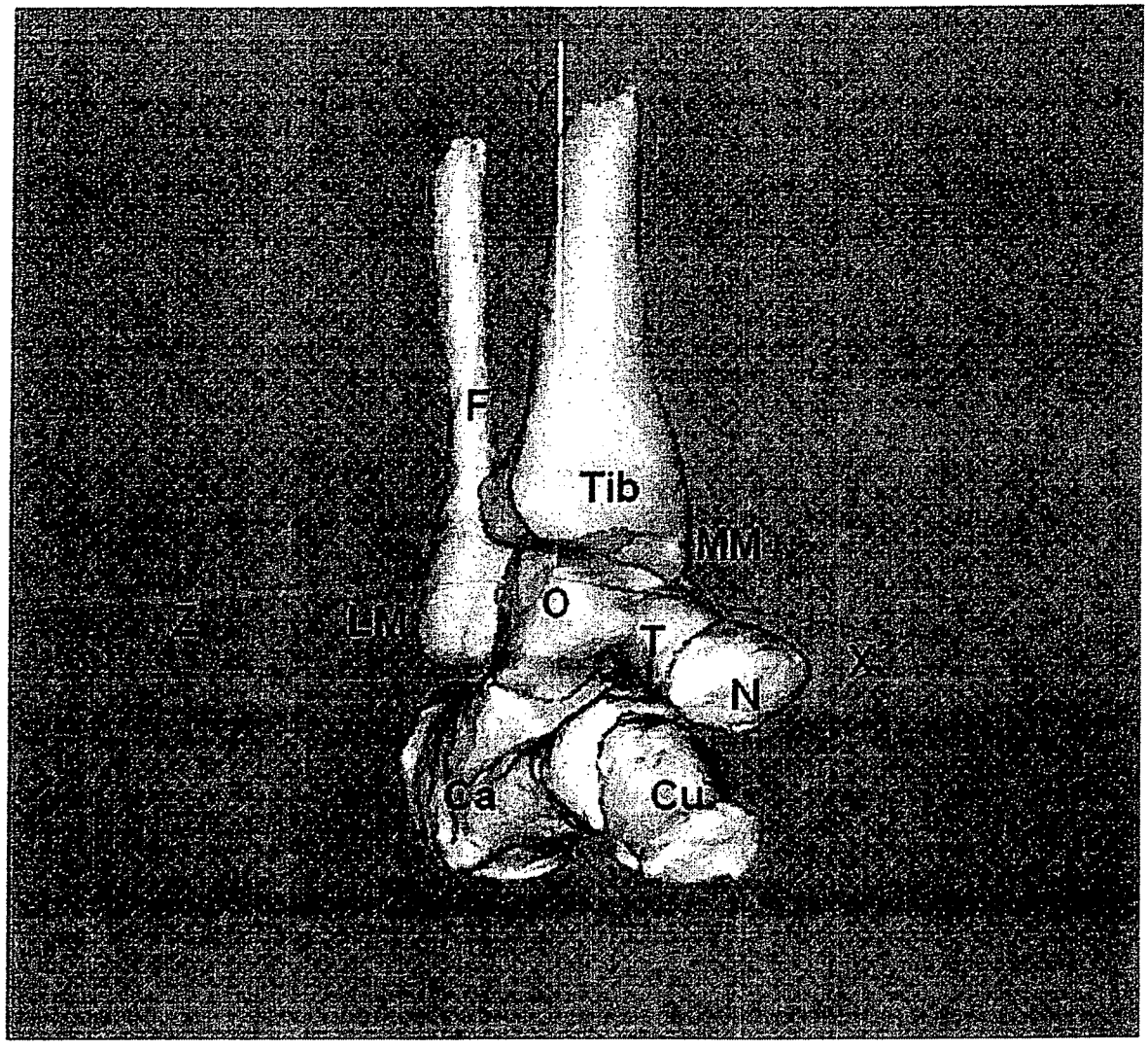

Figure 1. Establishing the standard coordinate system. Tib, tibia; F, fibula; T, talus; Ca, calcaneus; Cu, cuboid; N, navicular; O, origin; X, Y, and Z stand for the *x*-, *y*-, and *z*-axes of the standard coordinate system; LM, lateral malleoli; MM, medial malleoli.

the LCS was completed by the method of principal axes (x, y, z) and centroid (O). The principal axes were calculated by the software from the volume file and were orthogonal to each other and passing through the centroid. The position of the centroid plus the directions of the principal axes formed the mathematical representation and completely described the position and orientation of the bone in terms that could be further analyzed.[19] Because the orientation of the axes is dependent only on the shape of the bone surface, the LCS could be used as a set of markers attached to the bone.[20] However, the application of the LCS also depended on the stability of the principal axes within the bone. In other words, the principle axes should be stable within a bone regardless of whether the bone is normal or deformed by RA. Thus, the LCS could be used as a satisfactory marker set to analyze the displacement of the bone. Considering the dramatic change in shape of the bone surface in some RA patients, we modified the orientation of the axes using definite anatomical markers to make the axes more stable. The major principle axis was the basis of modification, because the major principal axis (long axis) was relatively stable and was used by Woodburn and colleagues to analyze hindfoot architecture in RA cases.[5] The origin and orientation of the LCS of each bone is shown in Figure 2.

For the calcaneus, the origin was the centroid of the calcaneus surface model, the x-axis was the long axis of the calcaneus in the forward direction, the z-axis lay in the plane defined by the x-axis and the centroid of the sustentaculum tali in the lateral direction, and the y-axis was perpendicular to the x-z plane in an upward direction. To obtain the centroid of the sustentaculum tali, the sustentaculum tali was cut off using unique

 DOI 10.1002/jor

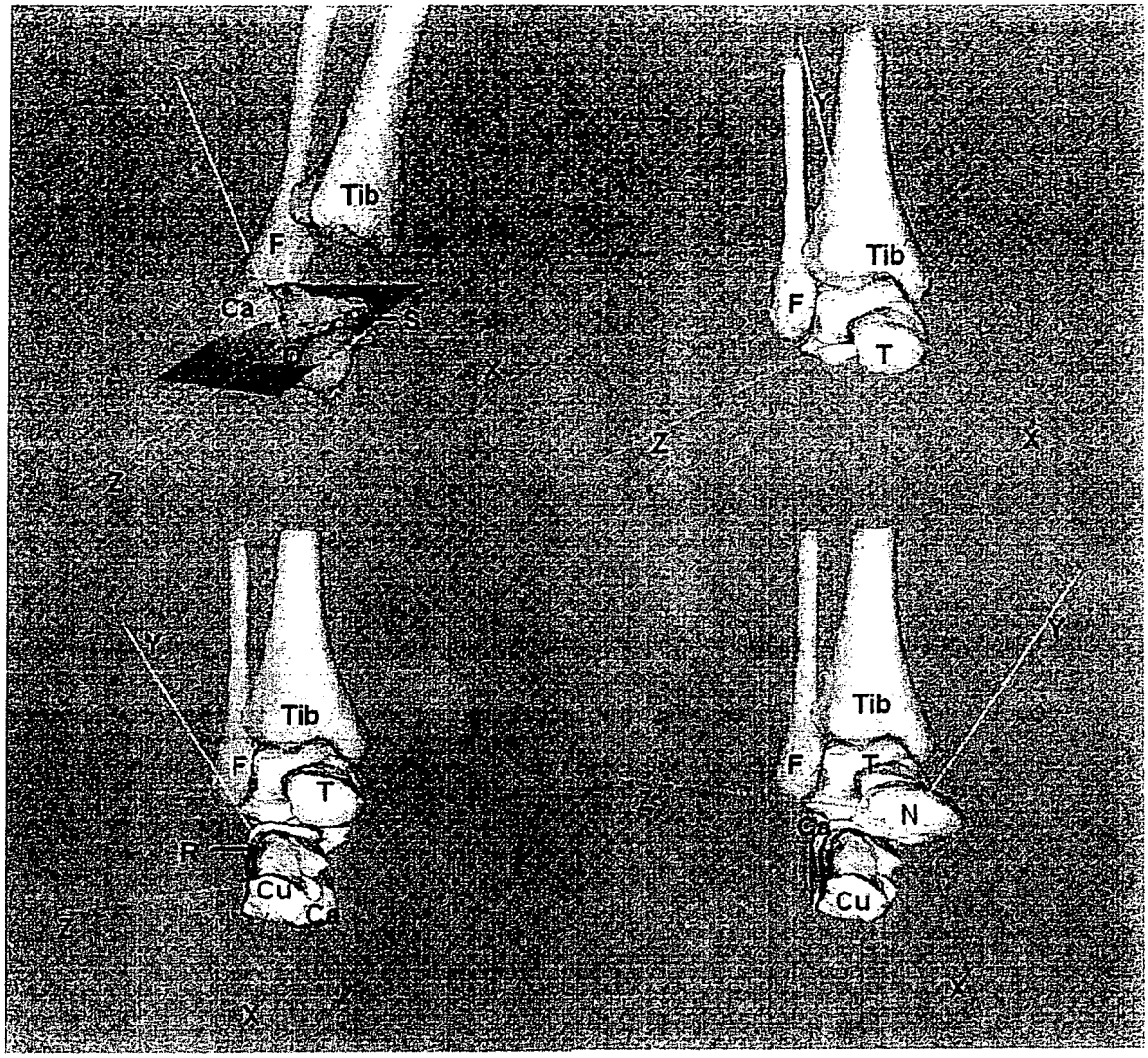

Figure 2. Establishing the local coordinate systems. Tib, tibia; F, fibula; T, talus; Ca, calcaneus; Cu, cuboid; N, navicular; R, ridge of the cuboid; S, sutentaculum tali of the calcaneus; O, origin is the centroid of the calcaneus surface model; X, Y, and Z stand for the X-, Y- and Z- axes of the local coordinate system.

software, and its bone model was reconstructed. The centroid position was determined by the software. The sustentaculum tali was then put back to its original position with the same software.

For the talus, the origin was the centroid of the talus surface model, the x-axis was the long axis of talus in the forward direction, the y-axis is perpendicular to the dome of the talus in an upward direction, and the z-axis was perpendicular to the x-y plane in a lateral direction. To determine the y-axis, a plane was passed through the centroid perpendicular to the x-axis. The line on the plane perpendicular to the dome of the talus was determined using unique software.

For the navicular, the origin was the centroid of the navicular surface model, the z-axis was the long axis of the navicular in a lateral direction, the y-axis was the middle axis with an upward direction, the x-axis was the shortest axis with a forward direction. The x-, y-, and z-axes were determined automatically by software calculations.

For the cuboid, the origin was the centroid of the cuboid surface model, the x-axis was the long axis of the cuboid in a forward direction, the y-axis passed through the ridge of the cuboid in an upward direction, and the z-axis was perpendicular to the x-y plane in a lateral direction. The ridge of the cuboid can be clearly identified from the bone model.

Once a stable LCS marker set was established for the talus, the centroid position and axes' orientation of the talus relative to the tibia (SCS) could be calculated. Three rotational parameters (Rx, Ry, Rz) and three translational parameters (Gx, Gy, Gz) were obtained by

the Eueler angle method. All translational parameters were normalized to the length between the LM and MM. By comparing the six parameters between groups, the displacement of the talus relative to the tibia was determined. A description of the displacement included the direction and amount of displacement of each bone's centroid, the orientation of rotation, and the amount of rotation.

The LCS matching method was used to analyze misalignments in the subtalar and midtarsal joints. The LCS of the RA talus was matched with that of the normal talus to analyze the displacements of the calcaneus and navicular in relation to the talus, which indicated the displacements in the subtalar and talonavicular joints, respectively. The LCS of the RA calcaneus was matched with that of the normal calcaneus to analyze the displacement of the cuboid relative to the calcaneus, which indicated the displacement in the cubocalcaneal joint. The LCS of the RA cuboid was matched with that of the normal cuboid to analyze the displacement of the navicular relative to the cuboid, which indicated the displacement in the cubonavicular joint.

The translational displacements along the *x*-, *y*-, and *z*-axes of the SCS were represented by *Gx*, *Gy*, and *Gz*, respectively. If any values increased in RA patients, the bone moved along the positive direction of the axis. Conversely, if any of these values decreased, the bone moved along the negative direction. *Rx*, *Ry*, and *Rz* denoted the rotational displacements around the *x*-, *y*-, and *z*-axes of the SCS, respectively. If these values increased in RA patients, the bone had varus rotation, adduction, and dorsal flexion, respectively. Conversely, if these values decreased, the bone showed valgus rotation, abduction, and plantar flexion.

The pattern of deformity was visualized using surface models created by a modified version of Visualization Toolkit software (Kitware Inc., New York, NY). The resulting calculated deformities were validated through animation made by the same software.

Validation of Accuracy

The accuracy of the methodology was determined in vitro. Three MR images and CT scans of a fresh cadaveric foot were acquired, only changing the direction of the MRI or CT slices. Segmentation and 3D reconstruction of the cuboid and calcaneus were conducted separately from each set of data, followed by the establishment of the LCSs of both bones. The relative position of the cuboid to the calcaneus was obtained using the LCS of each bone and compared among the three MRI or CT slices. The results in the MRI group showed a mean rotation error of $0.8° \pm 0.3°$ and a mean translation error of 0.04 ± 0.01 mm. In the CT group, the mean rotation error was $0.67° \pm 0.23°$ and the mean translation error was 0.03 ± 0.01 mm. Therefore, the experimental errors that might be caused by MRI or CT acquisition, segmentation, reconstruction, and establishment of an anatomical reference system were very small. The relative position of the cuboid to the calcaneus was also compared between the MRI and CT groups; the mean rotation error was $0.92° \pm 0.38°$, and the mean translation error was 0.08 ± 0.02 mm.

Statistical Analysis

Means and standard deviations were reported as descriptive statistics. A one-way MANOVA was conducted to determine if differences existed in the six parameters (*Gx*, *Gy*, *Gz*, *Rx*, *Ry*, and *Rz*) between the control and RA groups using SPSS software (ver. 12.0). A p value of less than 0.05 was considered significant.

RESULTS

Considering the displacement in the ankle joint (the talus relative to the tibia), the talus *Rz* decreased significantly ($p = 0.014$), so that the talus had plantar flexion relative to the tibia (Table 1). The rotation angle was 11° (Table 2, Fig. 3). For the displacements in the subtalar joint (the calcaneus relative to the talus) and the talonavicular joint (the navicular relative to the talus), the *Gy* and *Gz* of the calcaneus increased significantly ($p = 0.007$ and $p = 0.036$, respectively). The *Rx* of the calcaneus decreased significantly ($p < 0.0001$, Table 1). The increases of *Gy* and *Gz* demonstrated that the calcaneus translated laterally and upward in relation to the talus. The decrease of *Rx* indicated that the calcaneus had significant valgus rotation relative to the talus. The valgus angle was 10.5°, the lateral shift was about 3.9 mm, and the upward translation was 4.7 mm (Table 2, Fig. 3).

The *Rz*, *Gy*, and *Gz* of the navicular increased significantly ($p < 0.001$, $p = 0.001$, and $p = 0.002$, respectively). The *Rx* and *Ry* of the navicular decreased significantly ($p < 0.0001$ and $p = 0.006$, respectively; Table 1). The increases of *Rz*, *Gy*, and *Gz* indicated that the navicular flexed dorsally as well as translated upward and laterally in relation to the talus. The decreases of *Rx* and *Ry* demonstrated that the navicular had valgus rotation and abduction relative to the talus. The angles were 11.6° valgus rotation, 7.6° abduction, and 15.5° dorsal flexion. The upward and lateral translations were 4.3 mm and 4.8 mm, respectively (Table 2, Fig. 3).

For displacements in the cubocalcaneal joint (the cuboid relative to the calcaneus) and the cubonavicular joint (the navicular relative to the cuboid), the three translational parameters (*Gx*, *Gy*, and *Gz*) and the three rotational parameters (*Rx*, *Ry*, and *Rz*) of the cuboid relative to the calcaneus showed no significant differences

DOI 10.1002/jor

Table 1. Displacement of the Four Bones in the Hindfoot of Patients with Rheumatoid Arthritis

		RA ($n = 21$)		Normal ($n = 10$)		
	Parameters	Mean	SD	Mean	SD	p
Talus–tibia	*Gx* (mm)	7.8	1.9	8.0	1.9	0.86
	Gy (mm)	−8.3	2.3	−9.1	1.7	0.33
	Gz (mm)	−6.8	1.0	−7.4	0.5	0.08
	Rx (deg)	16.8	8.0	15.4	4.3	0.58
	Ry (deg)	27.9	7.8	31.0	3.0	0.22
	Rz (deg)	−34.1	14.1	−22.0	4.4	0.01*
Cal–talus	*Gx* (mm)	−7.9	3.9	−9.9	2.0	0.14
	Gy (mm)	−35.1	4.8	−39.8	2.2	0.007*
	Gz (mm)	9.7	5.3	5.8	2.7	0.04*
	Rx (deg)	8.7	6.6	20.5	6.3	< 0.0001*
	Ry (deg)	10.5	8.8	11.1	4.2	0.84
	Rz (deg)	20.4	10.9	15.2	4.1	0.16
Navi–talus	*Gx* (mm)	35.0	2.6	34.6	2.8	0.71
	Gy (mm)	−17.8	3.5	−22.2	2.3	0.001*
	Gz (mm)	−17.0	4.3	−21.9	2.4	0.002*
	Rx (deg)	−36.7	8.3	−21.5	7.1	< 0.0001*
	Ry (deg)	9.0	13.2	22.3	6.7	0.006*
	Rz (deg)	−24.8	6.6	−36.4	9.9	< 0.001*
Cubo–cal	*Gx* (mm)	37.7	1.8	39.0	3.5	0.18
	Gy (mm)	−38.5	3.1	−39.4	3.1	0.50
	Gz (mm)	5.2	2.5	3.8	2.0	0.110
	Rx (deg)	−6.5	7.3	−5.5	7.2	0.73
	Ry (deg)	−30.8	5.7	−28.6	5.6	0.33
	Rz (deg)	−25.7	10.4	−30.8	7.8	0.18
Navi–cubo	*Gx* (mm)	36.0	1.9	34.3	2.7	0.05
	Gy (mm)	−21.4	2.1	−22.1	2.6	0.40
	Gz (mm)	−20.4	1.3	−21.7	2.9	0.09
	Rx (deg)	−22.6	5.6	−21.6	6.9	0.66
	Ry (deg)	17.6	7.7	22.7	5.7	0.07
	Rz (deg)	−31.4	8.0	−36.2	9.7	0.16

Gx, *Gy*, *Gz* stand for the position of the centroid in SCS.
Rx, *Ry*, *Rz* stand for the rotational displacement of bone around the *x*-, *y*-, and *z*-axes of the SCS.
*p value shows significant difference.

between the two groups (all six p values > 0.05). No significant displacement was found in the cubocalcaneal joint of RA patients. The same results were obtained for the three translational (*Gx*, *Gy*, and *Gz*) and three rotational parameters (*Rx*, *Ry*, and *Rz*) of the navicular relative to the cuboid (all six p values > 0.05; Table 1), with no significant displacement in the cubonavicular joint of RA patients. Thus, the calcaneus, the cuboid, and the navicular might be displaced together in RA patients with RA and have no relative displacement among them (Fig. 4). All of the results above are shown in Animation 1.

Animation 1: The Talus showed planter flexion relative to the tibia. The calcaneus, cuboid, and navicular bones might have the same pattern of deformity.

DISCUSSION

The in vivo 3D technique used in this study could provide accurate, quantitative, readily visualized, and clinically meaningful information for skeletal misalignment of RA hindfoot valgus deformity. Although radiographic measurement is the usual method used to analyze RA hindfoot valgus deformity objectively, most previous studies concentrated on medial arch collapse and heel valgus deformity using 2D methods. Such analysis could not provide a complete 3D description of structural changes in the tarsal region of an RA foot. A few 3D studies have been conducted, but the parameters used were too complicated for use in clinical practice. In our study, translational and rotational displacements of each hindfoot bone was accurately

Table 2. Average Displacement from Normal Position to RA Displacement Position

		Rotation (deg)		Center of Gravity (mm)
Talus to tibia	*Rx*	4.4 varus	*Gx*	0.1 posterior
	Ry	0.3 abduction	*Gy*	0.8 upward
	Rz	11.0 plantar flexion*	*Gz*	0.6 lateral
Calcaneus to talus	*Rx*	10.5 valgus*	*Gx*	2.0 anterior
	Ry	2.2 abduction	*Gy*	4.7 upward*
	Rz	4.6 dorsal flexion	*Gz*	3.9 lateral*
Navicular to talus	*Rx*	11.6 valgus*	*Gx*	0.4 anterior
	Ry	7.6 abduction*	*Gy*	4.3 upward*
	Rz	15.5 dorsal flexion*	*Gz*	4.8 lateral*
Cuboid to calcaneus	*Rx*	1.5 valgus	*Gx*	1.3 posterior
	Ry	1.7 abduction	*Gy*	0.8 upward
	Rz	4.6 dorsal flexion	*Gz*	1.5 lateral
Navicular to cuboid	*Rx*	3.7 valgus	*Gx*	1.7 anterior
	Ry	2.5 abduction	*Gy*	0.7 upward
	Rz	5.1 dorsal flexion	*Gz*	1.3 lateral

*p value shows significant difference.

described. The six parameters (*Gx*, *Gy*, *Gz*, *Rx*, *Ry*, and *Rz*) obtained using this technique are relatively simple and practical. In addition, the animation permitted good visualization of the deformity pattern, which might be beneficial in understanding the deformity pathomechanism. The number of abnormal parameters and the extent to which they deviated from normal gave a composite measurement of the severity of the deformity. Furthermore, the pattern of misalignment and the extent of displacement could be used for preoperative planning and reasonable surgical treatment.

Our results also confirmed the pathomechanism of RA hindfoot valgus deformity. Pes planovalgus is the most frequent deformity of the RA middle and hindfoot.[1,6] Changes in the subtalar and talonavicular joints are believed to dominate.[4] The presumed pathomechanism seems to be stress-related mechanical changes resulting from weakened ligaments.[4] RA causes severe inflammation of the talonavicular joint and the tarsal sinus, on the deep surface of which the strong plantar calcaneonavicular ligament rests. Diffuse inflammation in these areas alters the statics of the foot as a whole.[6] When the medial arch does not tolerate weightbearing, 'the head of the talus falls down toward the medial side. . .in the plantar direction,'[2,6] and the calcaneus becomes deformed in a valgus direction, so the arch collapses and flatfoot occurs.

In our study, the talus flexed in the plantar direction, and the calcaneus showed a lateral, upward shift and valgus rotation. The displacements of the talus and calcaneus correspond to the pathomechanism described above. The stretch or disruption of the strongest interosseous ligament in the tarsal sinus should be considered.

Based on our results, talonavicular joint deformity and talar tilting may contribute to the mechanism of medial longitudinal arch collapse. Vanio believed that the break of the medial longitudinal arch is more frequent in the naviculocuneiform joint than in the talonavicular joint.[21] In contrast, Vahvanen described the talonavicular joint as the site of the crucial change producing flat foot and splay foot.[6] The navicular is elevated and displaced laterally, and consequently the head of the talus falls down towards the medial side of the foot in the plantar direction.[6] Gross and colleagues reported that navicular tuberosity displacement or drop may reflect excessive subtalar joint pronation, due to insufficient support of the medial longitudinal arch from ligaments and tendons.[22] Navicular displacement also indicates the degree to which the talus plantarly flexes in the space on the calcaneus that is stabilized during subtalar pronation.[23]

Our study is the first to report that the navicular bone showed valgus rotation, abduction, and dorsal flexion and translated upwardly and laterally relative to the talus. Combined with plantar flexion of the talus, the medial arch height decreased and medial bulging of the talonavicular joint occurred. The navicular tuberosity displacement or navicular drop was also seen using animation. Therefore, the talonavicular joint might be a key point of medial arch collapse. Further study on the

DOI 10.1002/jor